

Enhanced charge separation by interchain hole delocalization in nonfullerene acceptor-based bulk heterojunction materials

Chang-Mok Oh¹ | Sujung Park² | Jihoon Lee³ | Sung Heum Park³ | Shinuk Cho² | In-Wook Hwang¹ 

¹Advanced Photonics Research Institute, Gwangju Institute of Science and Technology, Gwangju, Republic of Korea

²Department of Physics and Energy Harvest Storage Research Center, University of Ulsan, Ulsan, Republic of Korea

³Department of Physics, Pukyong National University, Busan, Republic of Korea

Correspondence

Shinuk Cho, Department of Physics and Energy Harvest Storage Research Center, University of Ulsan, Ulsan 44610, Republic of Korea.

Email: sucho@ulsan.ac.kr

In-Wook Hwang, Advanced Photonics Research Institute, Gwangju Institute of Science and Technology, Gwangju 61005, Republic of Korea.

Email: hwangi@gist.ac.kr

Abstract

Bulk heterojunction (BHJ) composites show improved power conversion efficiencies when optimized in terms of morphology using various film processing methods. A reduced carrier recombination loss in an optimized BHJ was characterized previously. However, the driving force that leads to this reduction was not clearly understood. In this study, we focus on the decreased carrier recombination loss and its driving force in optimized nonfullerene acceptor-based PTB7-Th:IEICO-4F BHJ composites. We demonstrate that the optimized BHJ shows deactivation in the sub-nanosecond nongeminate carrier recombination process. The driving force for this deactivation was determined to be the improved interchain hole delocalization between the polymers. An enhanced interchain hole delocalization was observed using steady-state photoinduced absorption (PIA) spectroscopy. In particular, increased splitting between the polaron PIA bands was noted. Moreover, improved interchain hole delocalization was observed for other state-of-the-art BHJ materials, including D18:Y6 with optimized morphologies.

KEYWORDS

bulk heterojunction, interchain hole delocalization, nonfullerene acceptor, photoinduced absorption spectroscopy, solar cell

1 | INTRODUCTION

Recently, high-performance organic solar cells (OSCs) were fabricated using bulk heterojunction (BHJ) composites, comprising semiconducting polymer electron donors and small-molecule electron acceptors, to obtain high exciton dissociation yields by ultrafast photoinduced

electron and hole transfer processes.^{1–4} In BHJs, high efficiency of carrier generation and transport is realized by the bicontinuous network structures of the donor and acceptor aggregates. As bicontinuous networks are created by the self-assembly of organics, various processing methods for BHJ films, such as addition of processing additives (high-boiling-point solvents) to a donor–acceptor

Chang-Mok Oh and Sujung Park contributed equally to this study.

This is an open access article under the terms of the Creative Commons Attribution License, which permits use, distribution and reproduction in any medium, provided the original work is properly cited.

© 2023 The Authors. *Carbon Energy* published by Wenzhou University and John Wiley & Sons Australia, Ltd.

composite solution,^{5,6} solvent and additive soaking,^{7–9} thermal annealing (TA),¹⁰ and solvent vapor annealing (SVA),¹¹ have been successfully performed to optimize the morphology of BHJs. Optimization in the BHJ morphology is known to increase the carrier mobility^{5–11} and decrease the carrier recombination loss.^{3,4} However, the driving factor that deactivates the carrier recombination process was not clearly understood.

Compared to fullerene acceptor-based BHJs, nonfullerene acceptor-based BHJs are synthesized for improved photocurrent and voltage generation by utilizing extended photoabsorption to the near-infrared regime and small energy gaps between the lowest unoccupied and highest occupied molecular orbitals of the donor and the acceptor, respectively. Consequently, these materials showed improved power conversion efficiencies (PCEs) of up to 19% in recent OSCs.^{12–17} In nonfullerene acceptor-based BHJs, the excitons are efficiently dissociated by ultrafast (sub-picoseconds) electron and fast (few picoseconds) hole transfer processes.^{9,18–23} However, a drawback of the back electron transfer (BET) process in going from the electron acceptor to the donor, that is, the carrier recombination process, is the limited carrier generation and transport in nonfullerene acceptor-based OSCs.^{18,19,22–28} Therefore, deactivation of this energy loss process is important to improving PCEs.

In this work, we focused on the carrier generation and recombination processes in a high-performance nonfullerene acceptor-based BHJ, comprising the polymer electron donor PTB7-Th and the small-molecule nonfullerene electron acceptor IEICO-4F, and studied through photoinduced absorption (PIA) spectroscopy before and after morphology optimization using a processing additive.

In a previous study,²⁹ the PTB7-Th:IEICO-4F (1:1.5) composite showed significant improvement in its PCE from ~9% to >12% on optimizing the BHJ morphology through the addition of a processing additive (4 vol.% 1-chloronaphthalene [CN]) to a chlorobenzene (CB) solution containing PTB7-Th and IEICO-4F. Through space charge-limited current (SCLC) and grazing incidence wide-angle X-ray scattering (GIWAXS) analyses, Song et al.²⁹ demonstrated that the improvement in PCE is mainly attributed to the increased mobility of the electron (μ_e of 4.56×10^{-5} to 1.48×10^{-4} cm²/Vs) and hole (μ_h of 9.35×10^{-5} to 1.42×10^{-4} cm²/Vs), and increased π - π coherent length between the acceptors.

From the time-resolved and steady-state PIA spectroscopy data, we found that the enhanced PCE in the optimized PTB7-Th:IEICO-4F is ascribed to the decreased carrier recombination loss in sub-nanoseconds after photoexcitation, and its driving force is the carrier delocalization along the materials. The yield of the initial exciton dissociation after

photoexcitation shows negligible changes with the incorporation of an additive. However, BET, that is, delayed carrier recombination in sub-nanoseconds, was deactivated because of the improved interchain hole delocalization, as characterized by the shifts of the delocalized polaron PIA bands (DP₁ and DP₂) in the near- and mid-infrared regime of the steady-state PIA spectra.

The systematic energy shifts in the delocalized polaron PIA bands after the optimization of the BHJ morphology using different film processing methods (additive adding [AA], solvent and additive soaking, TA, and SVA) have been observed for other state-of-the-art nonfullerene acceptor-based BHJs (PBDB-T:ITIC-m, PM6:Y6, and D18:Y6). The results demonstrate the important role of the observed interchain hole delocalization in various nonfullerene acceptor-based BHJs. Thus, our findings provide new insights for optimizing the BHJ morphology by observing the interchain hole delocalization using steady-state PIA spectroscopy.

2 | RESULTS AND DISCUSSION

The chemical structures of PTB7-Th and IEICO-4F, current–voltage (J – V) characteristics, and incident-photon-to-electron conversion efficiency (IPCE) spectra of the devices fabricated using pristine and CN-treated PTB7-Th:IEICO-4F (1:1.5) BHJ films are shown in Figure 1A,B. To evaluate these materials, we fabricated inverted OSCs, comprising indium–tin–oxide (ITO)/ZnO/BHJ/MoO_x/Ag, and following details can be seen in previous publication (Supporting Information).²⁹ The CN-treated cell showed improved device parameters (PCE, fill factor [FF], short circuit current [J_{sc}], and open-circuit voltage [V_{oc}] of 12.7%, 70%, 25.8 mA/cm², and 0.706 V, respectively), compared with those of the pristine cell (PCE, FF, J_{sc} , and V_{oc} of 8.4%, 54%, 20.8 mA/cm², and 0.740 V, respectively), resulting in the enhanced photocurrent over the entire photoabsorption spectral range of 300–1000 nm. In addition, the device parameters of the CN-treated cell are consistent with previous results (PCE, FF, J_{sc} , and V_{oc} of 12.8%, 66%, 26.8 mA/cm², and 0.712 V, respectively).²⁹ The larger grain size distribution of the CN-treated BHJ than that of the pristine BHJ was also observed (Figure S1).

The steady-state absorption and photoluminescence (PL) spectra of the PTB7-Th, IEICO-4F, pristine, and CN-treated BHJ films are shown in Figure 1C. To characterize the exciton dissociation yields, we plotted the PL spectra after dividing their intensities by the absorption intensity at the excitation wavelength of 532 nm. In the BHJ, the PLs of PTB7-Th and IEICO-4F are quenched by

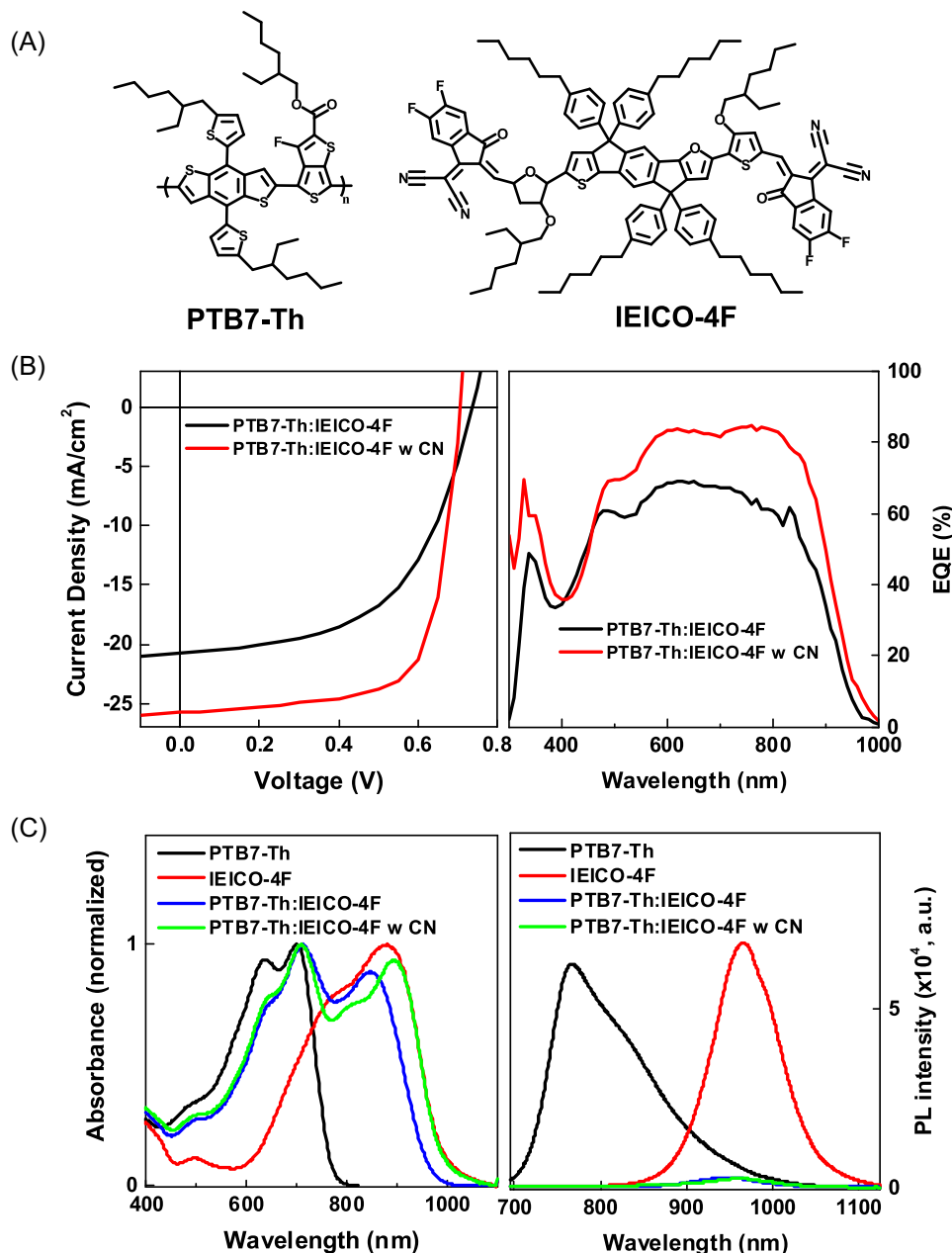


FIGURE 1 Device, absorption, and PL characteristics of the film. (A) Molecular structures of PTB7-Th and IEICO-4F, (B) current-voltage ($J-V$) and IPCE plots for the OSCs fabricated using pristine and CN-treated PTB7-Th:IEICO-4F films, and (C) absorption and PL spectra of the PTB7-Th, IEICO-4F, pristine, and CN-treated PTB7-Th:IEICO-4F films. The PL spectra are plotted after dividing their intensities by the absorption intensity at the excitation wavelength of 532 nm. CN, 1-chloronaphtalene; IPCE, incident-photon-to-electron conversion efficiency; OSC, organic solar cell; PL, photoluminescence.

~99% and ~96%, respectively, regardless of the CN treatment. This indicates the efficient and consistent exciton dissociation yields in the pristine and CN-treated BHJ films after photoexcitation.

To characterize the carrier generation and recombination processes, we measured the time-resolved PIA spectra and decay profiles of the PTB7-Th, IEICO-4F, pristine, and CN-treated BHJ films after photoexcitation at 630 nm, for example, pumping of the polymer and the

acceptor (Figures 2 and 3). The data were obtained at a low pump light intensity of $<2 \mu\text{J}/\text{cm}^2$, which does not cause bimolecular carrier annealing. The rise times, decay times, and relative amplitudes obtained from exponentially fitting the decay are listed in Table 1. At 1050 nm, PTB7-Th showed two time-decay components of 120 and 850 ps. The 120-ps component is attributed to the singlet exciton state of PTB7-Th based on the comparable decay times observed from the PL decay measurement (Figure S2). The 850-ps

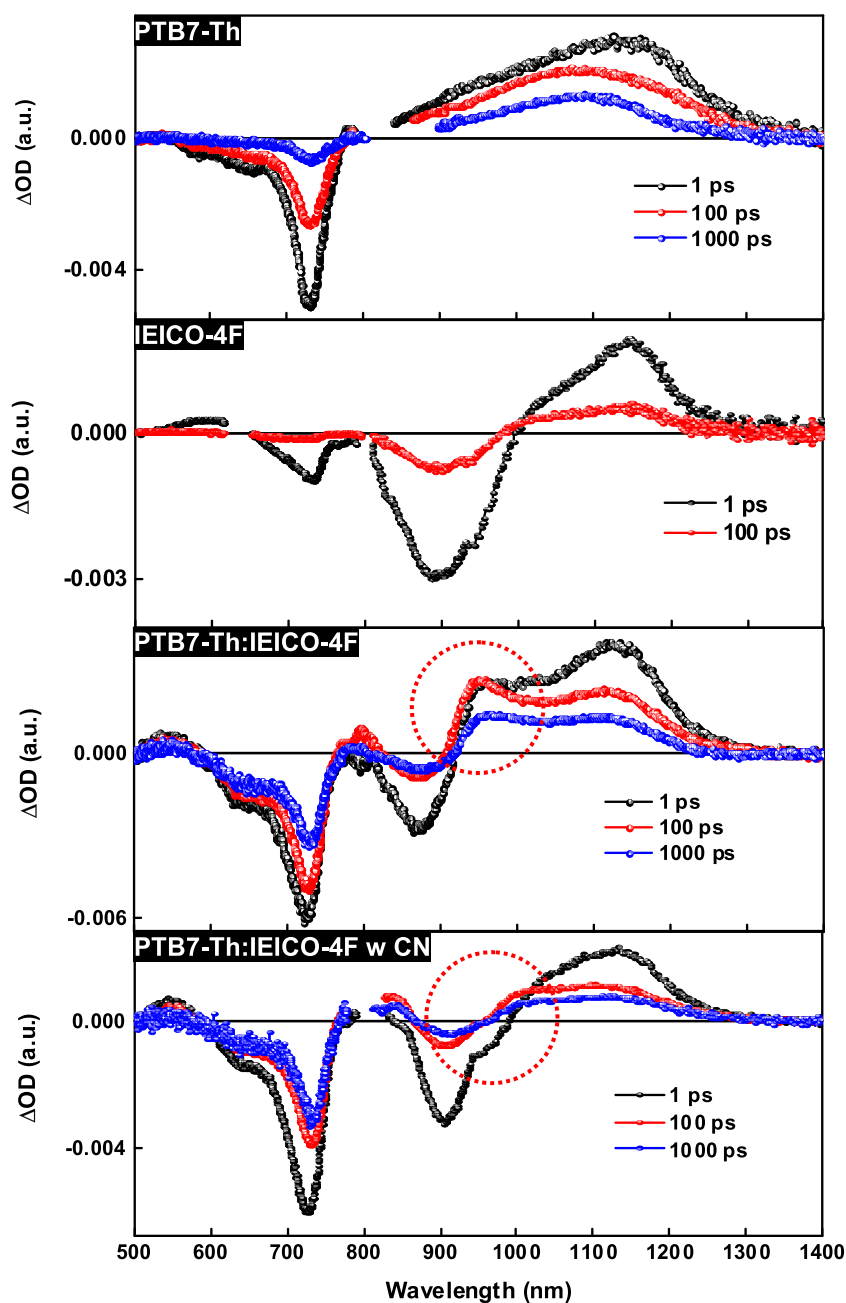


FIGURE 2 Time-resolved PIA spectra of the PTB7-Th, IEICO-4F, pristine, and CN-treated PTB7-Th:IEICO-4F films. The pump wavelength was 630 nm, and the intensity was $<2 \mu\text{J}/\text{cm}^2$. The PTB7-Th data were adopted from Oh et al.¹⁹ CN, 1-chloronaphthalene; PIA, photoinduced absorption.

component can be ascribed to the nonemissive polaron state of PTB7-Th. At 1050 nm, IEICO-4F showed a time-decay component of 180 ps, which is comparable with that observed from the PL decay measurement and attributed to the singlet exciton state of IEICO-4F (Figure S2).

The PIA spectra of the BHJ film showed two distinct PIA bands at ~ 950 and ~ 1150 nm (third panel in Figure 2). The initial 1-ps PIA band at ~ 1150 nm is consistent in shape with that observed in IEICO-4F, indicating its singlet exciton state. In contrast, the PIA band at ~ 950 nm is characteristic to PTB7-Th:IEICO-4F. By fitting the decay at 1120 nm, we observed the hole transfer times of 10 (46%) and 50 (10%) ps for the pristine BHJ film, and 10 (55%) and 36 (15%) ps for the

CN-treated BHJ film. During fitting, we used the time-decay components of 50 and 36 ps, which were observed from the PL decay measurement of the BHJ films (Figure S2). By obtaining the weight average of the time-decay components of 10, 36, and 50 ps, we calculated average hole transfer times of 17 and 16 ps for the pristine and CN-treated BHJ films, respectively. The observed similarity in the hole transfer time corresponds well with the consistent exciton dissociation yield of 96%, which was characterized by PL spectroscopy (Figure 1C). By fitting the decay at 1120 nm, the BHJ films showed PIA with a constant magnitude of more than 1 ns, which is a characteristic of long-lived mobile polarons.

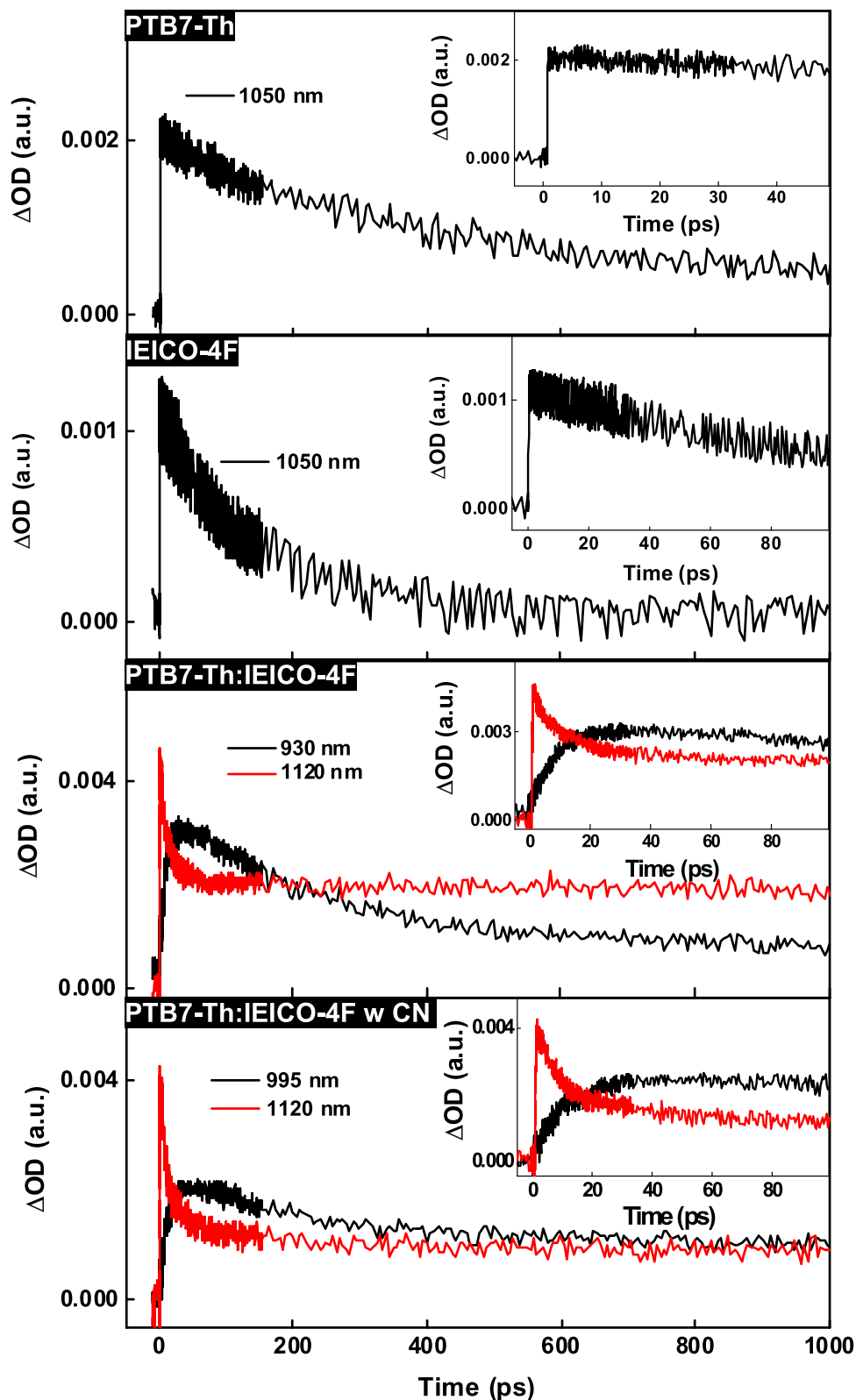


FIGURE 3 PIA decay profiles of the PTB7-Th, IEICO-4F, pristine, and CN-treated PTB7-Th:IEICO-4F films. The probe wavelengths are indicated in each panel. The pump wavelength was 630 nm, and the intensity was $<2 \mu\text{J}/\text{cm}^2$. The inset of each panel shows the signal decays at a short time scale. CN, 1-chloronaphthalene; PIA, photoinduced absorption.

TABLE 1 PIA decay parameters of the PTB7-Th, IEICO-4F, pristine, and CN-treated PTB7-Th:IEICO-4F BHJ films^a

Probe wavelength (nm)	Fitted decay times (ps)		
	τ_1	τ_2	τ_3
PTB7-Th			
1050	120 (25%)	850 (75%)	
IEICO-4F			
1050	180 (100%)		
Pristine PTB7-Th:IEICO-4F			
930	10 ^{rise}	250 (75%)	>1000 (25%)
1120	10 (46%)	50 (10%)	>1000 (44%)
CN-treated PTB7-Th:IEICO-4F			
995	10 ^{rise}	250 (53%)	>1000 (47%)
1120	10 (55%)	36 (15%)	>1000 (30%)

Abbreviations: CN, 1-chloronaphthalene; PIA, photoinduced absorption.

^aA pump wavelength of 630 nm and an intensity of $<2 \mu\text{J}/\text{cm}^2$ were used. The time decay constants were obtained by deconvoluting the measured signal decay from the pump beam time profile (characterized by a full-width at half-maximum of ~ 150 fs) and fitting to a sum of the exponential terms, that is, $\Delta\text{OD}(t) = A_1 \exp(-t/\tau_1) + A_2 \exp(-t/\tau_2) + A_3 \exp(-t/\tau_3)$, where $\Delta\text{OD}(t)$ is the time-dependent transient absorption intensity, A is the amplitude (normalized percentage $[A_i/(|A_1| + |A_2| + |A_3|) \times 100]$), and τ is the fitted decay time.

The ultrafast electron transfer in the BHJ films was characterized by transient absorption anisotropy (TAA) (Figure S3). That the TAA of the BHJ films pumped at 630 nm and probed at 1050 nm showed ultrafast time decay t_1 of ~ 265 fs. In contrast, the TAA of PTB7-Th and IEICO-4F showed a time decay t_1 of ~ 460 and ~ 160 fs, respectively. The observed decrease in the decay time from 460 to 265 fs indicates the ultrafast electron transfer from PTB7-Th to IEICO-4F after photoexcitation.

By fitting the 930-nm PIA decay of the pristine BHJ film, we determined the signal rise and decay with a time component of ~ 10 and ~ 250 ps, respectively. The time-decay component of 250 ps was systematically reduced to 72 ps by increasing the pump light intensity in the range of $2\text{--}20 \mu\text{J}/\text{cm}^2$ (Figure S4). The characteristics of the slow PIA rise, sub-nanosecond PIA decay, and strong PIA decay time dependence on the pump light intensity are consistent with those of other nonfullerene-acceptor-based BHJs (PBDB-T:ITIC-m and PTB7-Th:COi8DFIC), where these characteristics were attributed to the nongeminate charge-transferred (CT) states.^{18,19} In addition, Lee et al.³⁰ recently demonstrated that the 950-nm PIA band in PTB7-Th:IEICO-4F is ascribed to the bound polaron pairs

generated at the interface of the polymer and acceptor networks. This interpretation is based on the disappearance of this band in ternary PTB7-Th:IEICO-4F:PCBM composites, where PCBM is believed to decrease the interface area between PTB7-Th and IEICO-4F. In this work, we attributed the 950-nm PIA band to the nongeminate CT states composed of bound polaron pairs generated at the interface of the polymer and acceptor networks after photoexcitation and charge migration. Considering the short decay time of 250 ps, the 950-nm PIA band represents prompt carrier recombination after photoexcitation and charge migration.

Compared to the pristine BHJ film, the CN-treated BHJ film shows a drastic decrease in the relative amplitude of the 950-nm PIA band, resulting in a stimulated emission at ~ 950 nm (dotted circles in Figure 2). The PIA decays at 930 and 995 nm in the pristine and CN-treated BHJ films also showed a decreased relative amplitude of the 250-ps time-decay component. The decrease in the relative amplitude of the 950-nm PIA band in the CN-treated BHJ film corresponds with the significant decrease in the carrier recombination loss after photoexcitation and charge migration, which led to an improvement in J_{sc} and FF (Figure 1B).

To determine the driving factor for the decreasing carrier recombination loss in the CN-treated BHJ film, we measured the steady-state PIA spectra in the near- and mid-infrared regimes obtained at room temperature and -190°C (83 K), respectively. As shown in Figure 4, the BHJ films had two distinct PIA bands at the low- (0.1–0.4 eV) and high- (0.8–1.2 eV) energy regimes. During the transition from pristine to CN-treated BHJ films, red and blue shifts of the low- and high-energy PIA band were observed, respectively. Based on the previous PIA band assignments in the rrP3HT by Österbacka et al.,³¹ we could analyze the mechanism for these band shifts. The heterogeneity in the morphology of rrP3HT results in its multiple PIA transition bands. Among these, the PIA transition bands in the near- and mid-infrared regime, denoted P_2 and P_1 , respectively, are attributed to the interband and intraband transitions between the polaron energy states, as shown in Scheme 1. In the transition from the disordered to ordered morphology in rrP3HT, the high- and low-energy PIA band is blue- and red-shifted, respectively, because of the interchain coupling between the polaron energy states and dipole-allowed optical transitions, thereby achieving delocalized polaron PIA bands DP_2 and DP_1 , respectively.³¹ Therefore, the red and blue shifts in the low- and high-energy PIA bands in Figure 4, which are comparable to those of Österbacka et al.,³¹ denote the improved interchain

coupling between the polaron energy states and interchain polaron delocalization. Considering the efficient hole transfer process from the acceptor to the polymer after photoexcitation, the polarons observed in Figure 4 are assumed to be holes. Thus, the improved interchain hole delocalization decreased the carrier recombination loss through two competing processes, namely, the interchain hole delocalization along the polymer networks and hole transfer to the bound polaron pair state at the interface of the polymer and acceptor networks, as shown in Scheme 1. We note that, despite previous reports on

polaron delocalization in fullerene-based BHJs through electrochemically induced absorption spectroscopy,³² electron nuclear double resonance spectroscopy,³³ and transient absorption-decay profiles using three pulses,³⁴ the increased interchain hole delocalization observed by PIA spectroscopy in nonfullerene acceptor-based BHJs in this work is novel.

Previous SCLC measurement of CN-treated PTB7-Th:IEICO-4F showed enhanced electron and hole mobility. However, the GIWAXS result did not show an increased π - π coherent length between the polymers.²⁹ The broad band characteristics in the GIWAXS spectra may cause difficulty in observing subtle changes in polymer stacking. Nonetheless, the PIA spectra in Figure 4 clearly indicate the enhanced interchain hole delocalization by CN treatment, which is in good agreement with the SCLC results.

To calculate the transition energy between the polaron energy states, we performed Gaussian band fitting for the mid-infrared PIA spectra (Figure S5). Using four Gaussian functions, including two infrared active vibration dips³⁵ at 0.15 and 0.19 eV and a PIA band at ~ 0.4 eV, we determined DP₁ transition energies of 0.18 and 0.11 eV for the pristine and CN-treated BJJ films, respectively. The PIA band at ~ 0.4 eV may be attributed to an intrachain P₁ transition, as reported by Kahmann et al.³⁶ Using a band gap of 1.5 eV, and DP₁ transition energies of 0.18 and 0.11 eV, we calculated DP₂ transition energies of 1.28 and 1.14 eV in the pristine and CN-treated BJJ films, respectively, as indicated in Scheme 1.³¹ These calculated DP₂ transition energies are larger than the DP₂ peak positions in Figure 4. This discrepancy can be attributed to the huge difference in the signal intensity of the PIA and photobleaching (PB) bands. The significantly larger PB bands at 1.3–1.4 eV may decrease the DP₂ PIA band intensity at >1.2 eV,

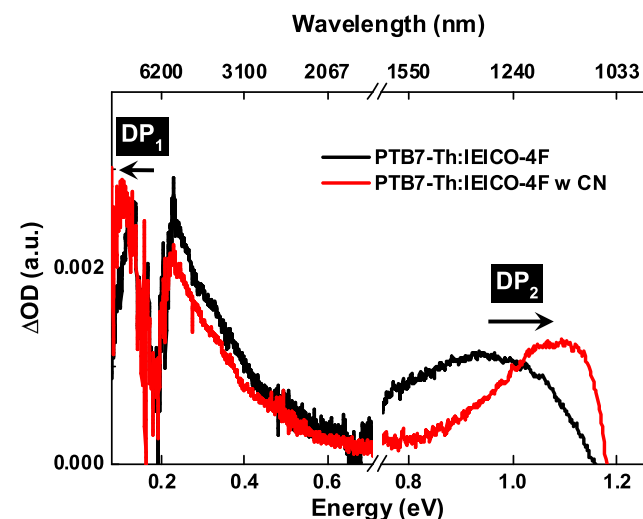
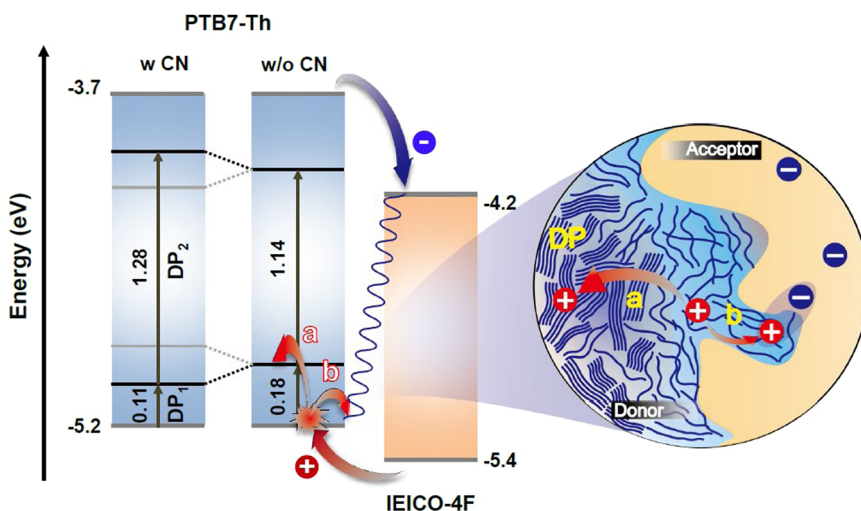


FIGURE 4 Steady-state PIA spectra of PTB7-Th:IEICO-4F. The near-to-mid-infrared regime of the PIA spectra was measured before and after the CN treatment on the PTB7-Th:IEICO-4F BJJ film. The pump wavelength was 532 nm, and the intensity was ~ 100 mW. The PIA spectra in the near- (0.7–1.2 eV) and mid-infrared (0.1–0.7 eV) regimes were obtained at room temperature and -190°C (83 K), respectively. CN, 1-chloronaphtalene; PIA, photoinduced absorption.

SCHEME 1 Energy diagram and schematic of the processes: (a) interchain hole delocalization and (b) nongeminate carrier recombination in PTB7-Th:IEICO-4F. The intraband and interband transition energies of the hole polarons, denoted DP₁ and DP₂, respectively, were obtained from the measurement of the steady-state PIA spectra. CN, 1-chloronaphtalene; PIA, photoinduced absorption.



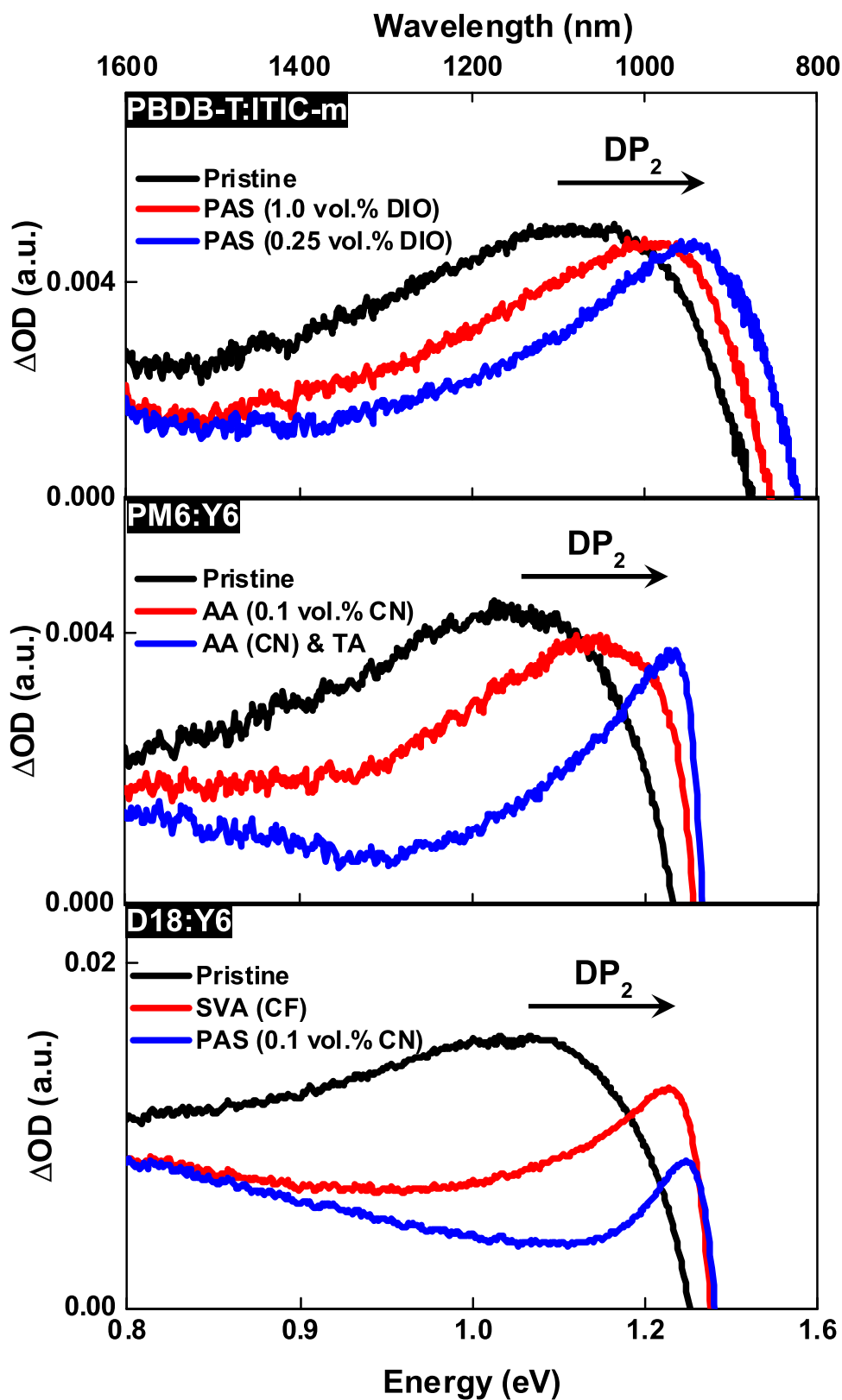


FIGURE 5 Steady-state PIA spectra of the state-of-the-art BHJ materials. The near-infrared regime PIA spectra of the PBDB-T:ITIC-m, PM6:Y6, and D18:Y6 films after the optimization of their BHJ morphologies using various film processing methods were obtained. The pump wavelength was 532 nm, and the intensity was ~ 100 mW. AA, additive adding; BHJ, bulk heterojunction; CF, chloroform; CN, 1-chloronaphthalene; PAS, postadditive soaking; PIA, photoinduced absorption; SVA, solvent vapor annealing; TA, thermal annealing.

thereby shifting the PIA peaks to a lower energy, as shown in Figure S6.

To investigate the impact of the interchain hole delocalization on the nonfullerene acceptor-based BHJs, we measured the steady-state PIA spectra for other state-of-the-art nonfullerene acceptor-based BHJs, namely, PBDB-T:ITIC-m, PM6:Y6, and D18:Y6. When optimizing the BHJ morphologies using different film processing methods, such as additive soaking for PBDB-T:ITIC-m,⁹ AA and TA for PM6:Y6,³⁷ and SVA for D18:Y6,³⁸ the high-energy DP₂ PIA bands at the near-infrared regime showed a blue shift (Figure 5). This indicates the important role of interchain hole delocalization in the optimal performance of nonfullerene acceptor-based BHJs, which can deactivate the carrier recombination loss processes after photoexcitation and charge migration.

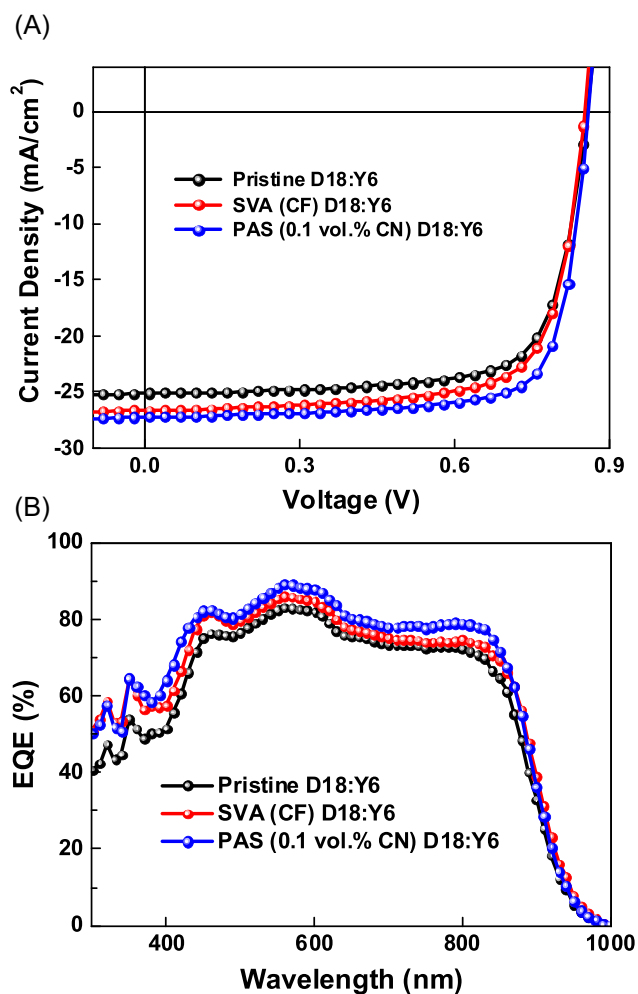


FIGURE 6 Device performance of the OSCs fabricated using D18:Y6. (A) Current-voltage ($J-V$) and (B) IPCE plots for the OSCs fabricated using pristine, SVA CF-treated, and PAS (0.1 vol.% CN)-treated D18:Y6 films. CF, chloroform; IPCE, incident-photon-to-electron conversion efficiency; OSC, organic solar cell; PAS, postadditive soaking; SVA, solvent vapor annealing.

Inspired by the effects of interchain hole delocalization in improving the PCE, we attempted to determine a larger blue shift of the DP₂ PIA band for the best-efficiency D18:Y6 by scanning solvent additives in the postadditive soaking (PAS) treatment.⁹ The PAS-treated D18:Y6 with 0.1 vol.% CN showed a larger blue shift of the DP₂ PIA band than that with conventional SVA (bottom panel in Figure 5). Subsequently, we fabricated an OSC with higher efficiency, as shown in Figure 6. The pristine and SVA-treated D18:Y6 showed lower PCEs than those in the literature owing to the device optimization and batch-to-batch dependence of the material syntheses.³⁸ However, the 0.1 vol.% CN PAS-treated D18:Y6 showed improved device parameters (PCE, FF, J_{sc} , and V_{oc} of 17.88%, 76.45%, 27.23 mA/cm^2 , and 0.86 V, respectively) than the control devices (PCE, FF, J_{sc} , and V_{oc} of 15.87%, 73.70%, 25.12 mA/cm^2 , and 0.86 V for the pristine BHJ; and 16.59%, 73.01%, 26.66 mA/cm^2 , and 0.85 V for the SVA-treated BHJ, respectively). This indicates that observing the infrared regime of the PIA spectra of nonfullerene acceptor-based BHJs is useful for improving their efficiency. We note that the film surface morphologies of the pristine and CN PAS-treated D18:Y6 do not show significant changes, as shown in Figure S7. Future studies will be focused on detailed characterization of PAS-treated D18:Y6 OSCs.

3 | CONCLUSION

In summary, from comparison of the ultrafast PIA spectroscopy data of pristine and CN-treated PTB7-Th:IEICO-4F BHJ films, we determined the nongeminate carrier recombination loss at the interface of the polymer and acceptor networks after photoexcitation and charge migration. Further, this loss was characterized by the decay time of ~ 250 ps, which was significantly deactivated by optimizing the BHJ morphology. From the steady-state PIA spectra in the near- to mid-infrared regime, the interchain hole delocalization between the polymers was drastically activated by optimizing the BHJ morphology, as confirmed by the blue and red shifts in the high- and low-energy polaron PIA bands DP₂ and DP₁, respectively. Subsequently, we demonstrated that the decrease in the carrier recombination loss is promoted by the enhanced interchain hole delocalization. In principle, the hole polarons generated after photoexcitation and charge migration alternatively moved into the bulk polymer networks or onto the interfacial bound polaron pair state. Therefore, the improved interchain hole delocalization reduced the carrier recombination loss at the interface. This was also observed for other state-of-the-art BHJ

materials (PBDB-T:ITIC-m, PM6:Y6, and D18:Y6) after optimizing their morphologies using different film processing methods. Thus, the critical role of interchain hole delocalization in nonfullerene acceptor-based BHJs was demonstrated. Finally, the PCE of D18:Y6-based OSCs was further increased by blue-shifting the DP₂ PIA band using 0.1 vol.% CN with PAS treatment, indicating that observing the PIA spectra is useful for finding better BHJ morphology.

ACKNOWLEDGMENTS

We would like to thank Editage (www.editage.co.kr) for English language editing. This work was supported by the National Research Foundation of Korea (NRF) grants funded by the Korea government (MSIT) (2022R1F1A1065586, 2019R1A6A1A11053838) and the GIST Research Institute (GRI) APRI grant funded by the GIST in 2022.

CONFLICTS OF INTEREST

The authors declare no conflicts of interest.

ORCID

In-Wook Hwang  <http://orcid.org/0000-0002-9314-2598>

REFERENCES

- Yu G, Gao J, Hummelen JC, Wudl F, Heeger AJ. Polymer photovoltaic cells: enhanced efficiencies via a network of internal donor-acceptor heterojunctions. *Science*. 1995;270(5243):1789-1791.
- Kraabel B, Lee CH, McBranch D, Moses D, Sariciftci NS, Heeger AJ. Ultrafast photoinduced electron transfer in conducting polymer-buckminsterfullerene composites. *Chem Phys Lett*. 1993;213(3,4):389-394.
- Hwang IW, Soci C, Moses D, et al. Ultrafast electron transfer and decay dynamics in a small band gap bulk heterojunction material. *Adv Mater*. 2007;19(17):2307-2312.
- Hwang IW, Moses D, Heeger AJ. Photoinduced carrier generation in P3HT/PCBM bulk heterojunction materials. *J Phys Chem C*. 2008;112(11):4350-4351.
- Peet J, Kim JY, Coates NE, et al. Efficiency enhancement in low-bandgap polymer solar cells by processing with alkane dithiols. *Nat Mater*. 2007;6(7):497-500.
- Lee JK, Ma WL, Brabec CJ, et al. Processing additives for improved efficiency from bulk heterojunction solar cells. *J Am Chem Soc*. 2008;130(11):3619-3623.
- Guo S, Cao B, Wang W, Moulin JF, Müller-Buschbaum P. Effect of alcohol treatment on the performance of PTB7:PC₇₁BM bulk heterojunction solar cells. *ACS Appl Mater Interfaces*. 2015;7(8):4641-4649.
- Kong J, Hwang IW, Lee K. Top-down approach for nanophase reconstruction in bulk heterojunction solar cells. *Adv Mater*. 2014;26:6275-6283.
- Choi H, Lee J, Oh CM, et al. Efficiency enhancements in non-fullerene acceptor-based organic solar cells by post-additive soaking. *J Mater Chem A*. 2019;7(15):8805-8810.
- Ma W, Yang C, Gong X, Lee K, Heeger AJ. Thermally stable, efficient polymer solar cells with nanoscale control of the interpenetrating network morphology. *Adv Funct Mater*. 2005;15(10):1617-1622.
- De Luca G, Treossi E, Liscio A, et al. Solvent vapour annealing of organic thin films: controlling the self-assembly of functional systems across multiple length scales. *J Mater Chem*. 2010;20(13):2493-2498.
- Zhu L, Zhang M, Xu J, et al. Single-junction organic solar cells with over 19% efficiency enabled by a refined double-fibril network morphology. *Nat Mater*. 2022;21(6):656-663.
- Cui Y, Xu Y, Yao H, et al. Single-junction organic photovoltaic cell with 19% efficiency. *Adv Mater*. 2021;33(41):2102420.
- Li S, Liu W, Li CZ, Shi M, Chen H. Efficient organic solar cells with non-fullerene acceptors. *Small*. 2017;13(37):1701120.
- Nielsen CB, Holliday S, Chen HY, Cryer SJ, McCulloch I. Non-fullerene electron acceptors for use in organic solar cells. *Acc Chem Res*. 2015;48(11):2803-2812.
- Hou J, Inganäs O, Friend RH, Gao F. Organic solar cells based on non-fullerene acceptors. *Nat Mater*. 2018;17(2):119-128.
- Chang L, Duan L, Sheng M, et al. Optimising non-patterned MoO₃/Ag/MoO₃ anode for high-performance semi-transparent organic solar cells towards window applications. *Nanomaterials*. 2020;10(9):1759.
- Oh CM, Lee J, Park SH, Hwang IW. Carrier losses in non-geminate charge-transferred states of nonfullerene acceptor-based organic solar cells. *Spectrochim Acta, Part A*. 2021;250:119227.
- Oh CM, Lee J, Park SH, Hwang IW. Enhanced charge separation in ternary bulk-heterojunction organic solar cells by fullerenes. *J Phys Chem Lett*. 2021;12(27):6418-6424.
- Zhong Y, Causa' M, Moore GJ, et al. Sub-picosecond charge-transfer at near-zero driving force in polymer:non-fullerene acceptor blends and bilayers. *Nat Commun*. 2020;11:833.
- Liu J, Chen S, Qian D, et al. Fast charge separation in a non-fullerene organic solar cell with a small driving force. *Nat Energy*. 2016;1(7):16089.
- Tamai Y, Fan Y, Kim VO, et al. Ultrafast long-range charge separation in nonfullerene organic solar cells. *ACS Nano*. 2017;11(12):12473-12481.
- Grancini G, Maiuri M, Fazzi D, et al. Hot exciton dissociation in polymer solar cells. *Nat Mater*. 2013;12(1):29-33.
- Awartani OM, Gautam B, Zhao W, et al. Polymer non-fullerene solar cells of vastly different efficiencies for minor side-chain modification: impact of charge transfer, carrier lifetime, morphology and mobility. *J Mater Chem A*. 2018;6(26):12484-12492.
- Wang J, Xie S, Zhang D, et al. Ultra-narrow bandgap non-fullerene organic solar cells with low voltage losses and a large photocurrent. *J Mater Chem A*. 2018;6(41):19934-19940.
- Shi J, Isakova A, Abudulimu A, et al. Designing high performance all-small-molecule solar cells with non-fullerene acceptors: comprehensive studies on photoexcitation dynamics and charge separation kinetics. *Energy Environ Sci*. 2018;11(1):211-220.
- Hinrichsen TF, Chan CCS, Ma C, et al. Long-lived and disorder-free charge transfer states enable endothermic charge separation in efficient non-fullerene organic solar cells. *Nat Commun*. 2020;11:5617.

28. Gillett AJ, Privitera A, Dilmurat R, et al. The role of charge recombination to triplet excitons in organic solar cells. *Nature*. 2021;597(7878):666-671.
29. Song X, Gasparini N, Ye L, et al. Controlling blend morphology for ultrahigh current density in nonfullerene acceptor-based organic solar cells. *ACS Energy Lett*. 2018;3(3):669-676.
30. Lee J, Lee JH, Yao H, et al. Efficient and photostable ternary organic solar cells with a narrow band gap non-fullerene acceptor and fullerene additive. *J Mater Chem A*. 2020;8(14):6682-6691.
31. Österbacka R, An CP, Jiang XM, Vardeny ZV. Two-dimensional electronic excitations in self-assembled conjugated polymer nanocrystals. *Science*. 2000;287(5454):839-842.
32. Matheson AB, Ruseckas A, Pearson SJ, Samuel IDW. Hole delocalization as a driving force for charge pair dissociation in organic photovoltaics. *Mater Horiz*. 2019;6(5):1050-1056.
33. Steyrlleuthner R, Zhang Y, Zhang L, et al. Impact of morphology on polaron delocalization in a semicrystalline conjugated polymer. *Phys Chem Chem Phys*. 2017;19(5):3627-3639.
34. Bakulin AA, Rao A, Pavelyev VG, et al. The role of driving energy and delocalized states for charge separation in organic semiconductors. *Science*. 2012;335(6074):1340-1344.
35. Miranda PB, Moses D, Heeger AJ. Ultrafast photogeneration of charged polarons in conjugated polymers. *Phys Rev B*. 2001;64(8):081201.
36. Kahmann S, Loi MA, Brabec CJ. Delocalisation softens polaron electronic transitions and vibrational modes in conjugated polymers. *J Mater Chem C*. 2018;6(22):6008-6013.
37. Yuan J, Zhang Y, Zhou L, et al. Single-junction organic solar cell with over 15% efficiency using fused-ring acceptor with electron-deficient core. *Joule*. 2019;3(4):1140-1151.
38. Liu Q, Jiang Y, Jin K, et al. 18% efficiency organic solar cells. *Sci Bull*. 2020;65(4):272-275.

SUPPORTING INFORMATION

Additional supporting information can be found online in the Supporting Information section at the end of this article.

How to cite this article: Oh C-M, Park S, Lee J, Park SH, Cho S, Hwang I-W. Enhanced charge separation by interchain hole delocalization in nonfullerene acceptor-based bulk heterojunction materials. *Carbon Energy*. 2023;5:e302. doi:10.1002/cey2.302